

Tunable Dirac points and zero-energy modes in periodic curved graphene superlattices

Jianli Luan,¹ Shangyang Li,¹ Tianxing Ma,^{1,2,*} Li-Gang Wang,^{3,†} and Hai-Qing Lin²

¹Department of Physics, Beijing Normal University, Beijing 100875, China

²Beijing Computational Science Research Center, Beijing 100193, China

³Department of Physics, Zhejiang University, Hangzhou 310027, China

(Dated: January 6, 2022)

We combined periodic ripples and electrostatic potentials to form curved graphene superlattices and studied effects of space-dependent Fermi velocity induced from curvature on their electronic properties. With the equal periods and symmetric potentials, Dirac points would not move but their locations will shift under asymmetric ones. This shift can be tuned by curvature and potentials. Tuneable extra gaps in band structures can appear with unequal periods. The existence of new Dirac points is discussed and these new Dirac points can appear under smaller potentials with curvature, and their locations can be changed even under fixed potential by adjusting curvature. Our results suggest that curvature provides a new possible dimension to tune the electronic properties in graphene superlattices and a platform to study physics near new Dirac points more easily.

INTRODUCTION

Graphene has attracted amounts of researches since it was realized experimentally in 2004 [1]. Its valance and conductance band touch at Dirac points (DPs). Near DPs, energy bands have linear dispersion and electrons can be described by massless Dirac equations [2].

Graphene superlattices (GSLs) have also been investigated theoretically and experimentally. GSLs can be realized by applying periodic [3–10], aperiodic [11–13] or disordered [14] electrostatic potentials, magnetic fields [15, 16], combination of them [17, 18] and strains [19] on graphene. In these structures, people find new DPs [4–9] and anisotropy Fermi velocity [3–7] etc. These novel properties can be used to investigate electron's motion in it, such as *Zitterbewegung* [20] and Bloch oscillation [12]. Building periodic structures, such as periodic corrugated graphene [21], Moiré patterns [22] and heterosubstrate [23], is another method to induce GSLs. In particular, Moiré superlattice formed by twisted bilayer graphene is attractive in these years due to its novel superconductivity [24, 25]. Since GSLs can tune electronic properties effectively, they may have giant applications in electronic or optical devices.

As a two-dimensional material, graphene exhibits intrinsic ripples to maintain its stability [26]. Controllable periodic corrugated graphene [27–33] has also been fabricated recently. This curvature can play significant roles on electronic structures [2, 34, 35], so it is possible to use it to control electronic properties. There are two widely used theoretical approaches to model Hamiltonian of curved graphene. One of them is quantum field theory in curved spacetime [36–42]. This method is on the basis of that low-energy electron in graphene can be described by massless Dirac equation and graphene is regarded as a continuum object. One can get Hamiltonian by combining Dirac equation and metric in curved surface [34]. By this way, such as topological defects [36] and helicoidal

graphene [40, 41] are investigated, and space-dependent Fermi-velocity is derived [36, 37]. The other way is tight-binding model with taking account of hopping's change caused by displacements of carbon atoms and strain [21, 43–45]. It successfully predicts the pseudo magnetic field [43, 44, 46]. However, both of them have weakness in roundly describing the curvature's effects, so other theories were developed, such as considering strain into metric [37, 42, 47], using discrete differential geometry [48], employing metric in reciprocal space [49] and rewriting Dirac equation to include strain [50]. In a word, space-dependent Fermi velocity and pseudo magnetic field are the most prominent impacts of curvature.

In this paper, periodic curved graphene superlattices (CGSLs) are constructed by applying electrostatic potentials on curved graphene and their electronic band structures are investigated. Here we mainly concentrated on space-dependent Fermi velocity's effects so we used one-dimensional sinusoidal surface to model curved graphene and Dirac equation in curved spacetime to obtain Hamiltonian. Due to the realization of controllable curved graphene [27–31, 33] and GSLs [9, 22], our proposal may be realizable experimentally.

CGSLs have two periodic structures (i.e. curved surface and potential). We first study the case of equal periods and symmetric potentials. The locations of original DPs are robust against curvature, but the band structures' slope near original DP (i.e. Fermi velocity) in both directions of along and perpendicular to potential wells decrease. That brings characteristics of new DPs [6, 7] into original ones. Nevertheless, the DPs can shift in asymmetric potentials and their displacements can be changed by adjusting curvature and potentials. Tuneable extra gaps can also exist with larger periods of curved surfaces. In addition, zero-energy modes [6, 7] and existence of new DPs are studied in detail. New DPs can appear with smaller potential due to the space-dependent Fermi velocity. The locations of them are

also tunable. Since the intrinsic nature of curvature in graphene, such effects may be not able to be neglected in experiments. With their prominent roles on electronic properties, CGSLs can have wide potential in application or some research on new DPs and transport in GSLs.

MODEL AND METHOD

The low-energy electronic state in monolayer flat graphene is described by massless Dirac equation, and its Hamiltonian reads [51]

$$H = \hbar v_f (k_x \sigma_x + k_y \sigma_y), \quad (1)$$

where $v_f = 10^6 \text{m/s}$ is Fermi velocity, σ_x and σ_y are Pauli matrices, and $\vec{k} = (-i \frac{\partial}{\partial x}, -i \frac{\partial}{\partial y})$ is the wave vector from K point.

Now we turn to curved case. Above discussions have stated that space-dependent Fermi velocity and pseudo magnetic fields are two main affects of curvature. Here we mainly focus on effects of the former, so we choose Dirac equation in curved spacetime. This method does not need to consider ripples extend in armchair or zigzag direction, which is convenient to apply potentials and in the view of experiments [40].

We rewrite Dirac equation into covariant form to obtain it in curved spacetime and Hamiltonian with the method proposed by previous research [34]. In this paper, we consider a one-dimensional periodic curved surface, which refers to that the ripples are only dependent on one coordinate and are written as $z = h(x)$. The line elements read

$$\begin{aligned} ds^2 &= dx^2 + dy^2 + dz^2 = dx^2 + dy^2 + \left(\frac{dz}{dx}\right)^2 dx^2 \\ &= (1 + g^2(x)) dx^2 + dy^2, \end{aligned} \quad (2)$$

with $g(x) = \frac{dz}{dx} = h'(x)$, so the metric is

$$g_{\mu\nu} = \text{diag}(1, -(1 + g^2(x)), -1). \quad (3)$$

After calculations described in Appendix A, we obtain Hamiltonian of graphene in this shape as

$$H = -i\hbar v_f \left(\frac{\sigma_x \partial_x}{\sqrt{1 + g^2(x)}} + \sigma_y \partial_y \right). \quad (4)$$

Comparing Eq. (1) with (4), we find that graphene gets space-dependent decreased Fermi velocity in x -direction.

Since we do not take account of discreteness of lattice and strain induced by ripples and spin connection [34] is zero in one-dimensional curved surface, our Hamiltonian can not include the pseudo magnetic field in curved graphene. However, we only concern about Fermi velocity and low-energy electronic states here, and GSLs are also continuum objects and their lengths are larger

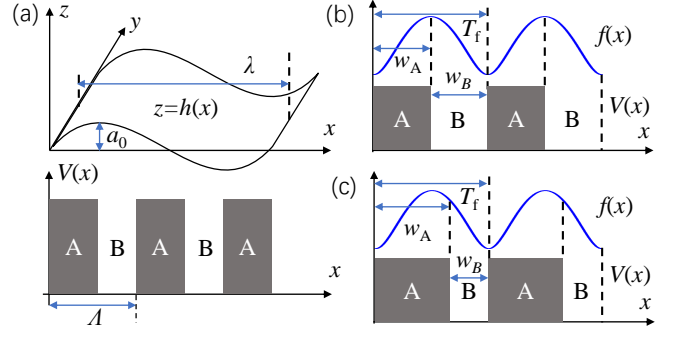


FIG. 1. (Color online) (a) Schematic of one-dimensional sinusoidal curved graphene and periodic potentials with square barriers. (b) is profiles of $f(x)$ and symmetric potentials. Here $w_A = w_B$ and $T_f = \Lambda$. The $f(x)$ has the same values in A or B regions. (c) is the asymmetric case $w_A > w_B$, and $f(x)$ in A has larger values than B region.

than deformation of lattices. This method is also appropriate to any ripple directions and more convenient to considering applied potentials. Besides, the tight-binding method can not reveal Fermi velocity's variation [43]. Although other modified methods can take account of other effects and derive other forms of Fermi-velocity [37, 50], they are only different from ours in specific values. Thus, our concise model can still reveal influences of renormalized Fermi velocity well and fits this paper's concerns.

In previous experimental research, controllable curved graphene has been realized [27–31, 33] and can be described by one-dimensional sinusoidal functions well [29]. Hence we use one-dimensional function $z = h(x) = a_0 \cos(\alpha x)$ to model curved graphene here with a_0 and $\lambda = \frac{2\pi}{\alpha}$ representing amplitude and period of it respectively. The Hamiltonian can be written from Eq. (4) as

$$\begin{aligned} H &= -i\hbar v_f \left(\frac{\sigma_x \partial_x}{\sqrt{1 + a_0^2 \alpha^2 \sin^2(\alpha x)}} + \sigma_y \partial_y \right) \\ &= -i\hbar v_f \left(\frac{\sigma_x \partial_x}{f(x)} + \sigma_y \partial_y \right), \end{aligned} \quad (5)$$

where $f(x) = \sqrt{1 + a_0^2 \alpha^2 \sin^2(\alpha x)}$ represents the effect of this curvature. The period of $f(x)$ is $T_f = \frac{\lambda}{2}$. When $a_0 = 0$ then $f(x) = 1$ and Hamiltonian (4) degrades into (1).

Then we apply one-dimensional periodic potentials $V(x)$ with square barriers on sinusoidal graphene and assume it is infinite in y -direction to obtain CGSL. The schematic of this CGSL is shown in Fig. 1. These potentials have AB structure with constant value inside each part and widths are indicated by w_A and w_B . Thus, here are two periods in our model (i.e. T_f and period of potentials $\Lambda = w_A + w_B$), and the lattice constant T of

a supercell in CGSL is the lowest common multiple of them.

Since scalar potentials in curved graphene can be added directly to Hamiltonian [52], we have total Hamiltonian

$$H = -i\hbar v_f \left(\frac{\sigma_x \partial_x}{f(x)} + \sigma_y \partial_y \right) + V(x)I, \quad (6)$$

with 2×2 unit matrix I . This Hamiltonian acts on two-component pseudospin wave function $\Psi = (\tilde{\psi}_A, \tilde{\psi}_B)^T$, and $\tilde{\psi}_{A,B}$ indicate smooth enveloping functions for A and B sublattice in graphene [8]. $\tilde{\psi}_{A,B}$ are written as $\psi_{A,B} e^{ik_y y}$ because of translation invariance.

To solve eigenequation of H , we need to obtain transfer matrix in the way constructed by [8]. The main problem of this model is that $f(x)$ is a continuous function, so it is not constant in the m th potential. Therefore, we divided the m th potential into n parts with extremely small width. Then we can regard $f(x)$ as constant in each small part and use the value at the midpoint of j th part f_j to represent it. After this approximation, the transfer matrix connects wave function from x to $x + \Delta x$ in the j th part reads

$$M_j(\Delta x, E, k_y) = \begin{pmatrix} \frac{\cos(q_j \Delta x - \theta_j)}{\cos \theta_j} & i \frac{\sin(q_j \Delta x)}{\cos \theta_j} \\ i \frac{\sin(q_j \Delta x)}{\cos \theta_j} & \frac{\cos(q_j \Delta x + \theta_j)}{\cos \theta_j} \end{pmatrix}. \quad (7)$$

Although it has the same expression with flat graphene [8], the parameters in it are totally different, which reflect the effects of potentials and curvature (see below). In Eq. (7), θ_j represents incident angle of wave functions and $\sin \theta_j = \frac{k_y}{k_j}$, $\cos \theta_j = \frac{q_j}{f_j k_j}$ with the wave vector $k_j = \frac{E - V_j}{\hbar v_f}$ and satisfying the relation $(f_j k_j)^2 = (q_j)^2 + (f_j k_y)^2$. Hence, q_j indicates x -component of wave vector and reads

$$q_j = \begin{cases} \text{sgn}(k_j) \sqrt{(f_j k_j)^2 - (f_j k_y)^2}, & k_j^2 > k_y^2 \\ i \sqrt{(f_j k_y)^2 - (f_j k_j)^2}, & \text{otherwise} \end{cases}. \quad (8)$$

The f_j reflects the influences of curvature and Eq. (7) is also valid for flat situation when $f_j = 1$. For the case of $k_y = 0$, Eq. (7) should be replaced by

$$M_j(\Delta x, E, k_y) = \begin{pmatrix} e^{f_j k_y \Delta x} & 0 \\ 0 & e^{-f_j k_y \Delta x} \end{pmatrix}. \quad (9)$$

The determinants of above matrices both fit $\det[M_j] = 1$. Detailed parameters and processes for deriving transfer matrix can also be found in Appendix B. Then we can find that the transfer matrix connects the two terminals of the m th potential should be

$$M_m(w_m, E, k_y) = \prod_{j=1}^n M_j(w_j, E, k_y), \quad (10)$$

where n is the total number of divided small parts in m th potential.

For an infinite CGSL system $(AB)^N$ with $N \rightarrow \infty$, the electronic dispersion at any incident angle can be calculated from Bloch's theorem

$$\cos(\beta_x T) = \frac{1}{2} \text{Tr} \prod_{i=1}^{T/\Lambda} (M_A M_B), \quad (11)$$

where T is lattice constant of CGSL, Λ is period of potentials and β_x is x -component of Bloch wave vector of the whole system. This relation is influenced by two periods Λ and T_f , and one can find their roles on electronic bands later. If there is a real solution of β_x , an electron or hole state will exist in band structure, otherwise band structure will show energy gap. According to this, we can obtain band structures discussed later and find the locations of DPs.

The transport properties for a finite superlattice $(AB)^N$ system can also be calculated by Eq. (7). We obtain the electronic reflection and transmission amplitudes from the continuity of wave functions [8] with the property of $\det[M_j] = 1$ as follows

$$r(E, k_y) = \frac{x_{22} e^{i\theta_0} - x_{11} e^{i\theta_e} - x_{12} e^{i(\theta_0 + \theta_e)} + x_{21}}{x_{22} e^{-i\theta_0} + x_{11} e^{i\theta_e} - x_{12} e^{i(\theta_e - \theta_0)} - x_{21}}, \quad (12)$$

$$r(E, k_y) = \frac{2 \cos \theta_0}{x_{22} e^{-i\theta_0} + x_{11} e^{i\theta_e} - x_{12} e^{i(\theta_e - \theta_0)} - x_{21}}, \quad (13)$$

where θ_0 and θ_e are incident and exit angle through the superlattice respectively. x_{ij} is the elements of the entire transfer matrix $X = \prod_{m=1}^N M_m(w_m, E, k_y) = \prod_{m=1}^N \prod_{j=1}^n M_j(w_j, E, k_y)$. Then the transmission probability reads $T = |t|^2$. These transport properties of finite systems are another reflection of band structures in infinite ones.

RESULTS AND DISCUSSION

In this section, we would like to calculate the band structures of periodic CGSLs from above model to discuss effects of space-dependent Fermi velocity induced by curvature. We focus on the location of DPs, effective Fermi velocity and appearance of new DPs. To make our results more realistic, we will choose realizable amplitude and period of curved graphene in experiments. There are two kinds of curved graphene in experiments. One of them has amplitude and period with nanometer length [27] and the other has amplitudes in 0.7nm-30nm and periods in 370nm-5 μ m [29]. For convenience, we choose amplitude a_0 and period λ that are in the same order of magnitude with the latter case (i. e. a_0 is of order 10nm and λ is of order 10²nm) in our calculation.

We firstly considered the case for that the potential and $f(x)$ have the same periods, which refers to $T_f = \Lambda$, and

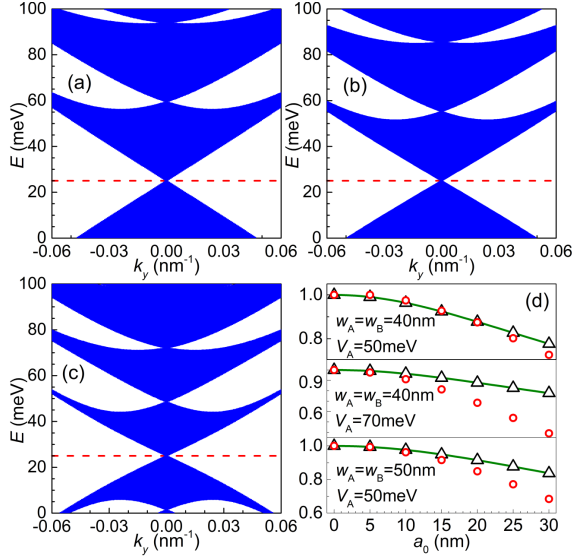


FIG. 2. (Color online) Electronic band structures for $a_0 = 0$ (a), $a_0 = 15\text{nm}$ (b) and $a_0 = 30\text{nm}$ (c). Here $V_A = 50\text{meV}$, $V_B = 0$, $w_A = w_B = 30\text{nm}$ and $T_f = \Lambda = w_A + w_B$. The red dashed lines denote the locations of DPs associated with $\text{zero-}\bar{k}$ gap. The black triangle and red circle drops in (d) denote the values of $\frac{v_x}{v_f}$ and $\frac{v_y}{v_f}$ respectively with different $w_{A,B}$ and V_A . The green lines in (d) exhibit the value of $1/\overline{f(x)}$. Here $V_B=0$ and $T_f = \Lambda$.

symmetric potentials with $w_A = w_B$. Here, we choose $V_A = 50\text{meV}$, $V_B = 0$ and $w_A = w_B = 30\text{nm}$, so the periods of curved surface and $f(x)$ are $\lambda = 120\text{nm}$ and $T_f = \frac{\lambda}{2} = 60\text{nm}$ respectively.

Figs. 2 (a)(b)(c) show band structures of CGSLs with $a_0 = 0, 15, 30\text{nm}$ respectively. From these bands, one can first find that the locations of DPs associated with $\text{zero-}\bar{k}$ gap [8] are 25meV and robust with different a_0 . This is originated from that potentials are symmetric and $\Lambda = T_f$, so $f(x)$ has the same values in the A or B potential, which is the case shown by Fig. 1(b), and will also be discussed in detail by a simplified model later. However, with increasing a_0 , the locations of other touching points of subbands with higher or lower energies are shifted and closer to the one at 25meV . The widths of gaps associated with them and all subbands also decrease simultaneously. This is due to the decreased slope of energy bands in k_y -direction with increasing a_0 . Meanwhile, the band structures' slopes in k_x -direction also decrease obviously when $a_0 \neq 0$, even though near the DP with $\text{zero-}\bar{k}$ gap. This property means that effective Fermi velocity will decrease in both x - and y -direction near original DPs in CGSLs, and is completely different from flat GSLs, since near original DPs in flat GSLs the x -direction Fermi-velocity is unchanged [6, 7]. One can also find this property from the Hamiltonian Eq. (4). These results suggest that space-dependent Fermi-velocity induced by curvature works on band structures

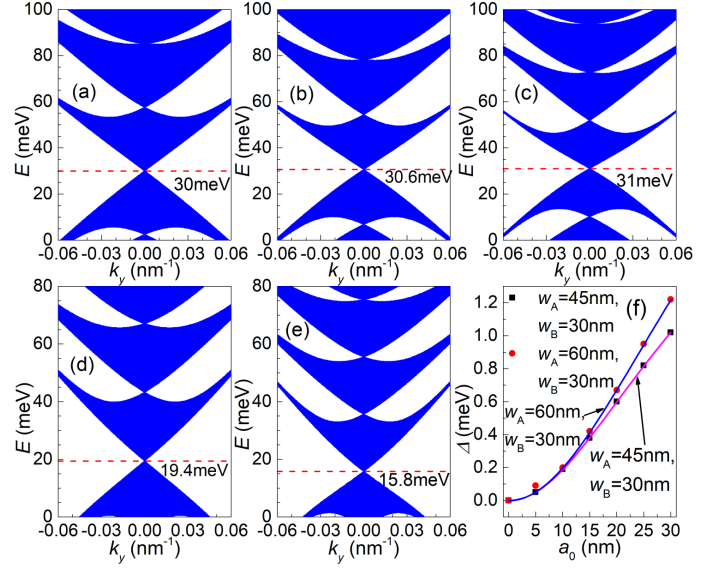


FIG. 3. (Color online) (a)-(e) Band structures under asymmetric potentials. $w_A = 45\text{nm}$, $w_B = 30\text{nm}$ in (a)-(c), $w_A = 30\text{nm}$, $w_B = 45\text{nm}$ in (d) and $w_A = 30\text{nm}$, $w_B = 60\text{nm}$ in (e). The amplitude of curved surface $a_0 = 0, 20\text{nm}$ and 30nm in (a)-(c) respectively. In (d) $a_0 = 20\text{nm}$ and in (e) $a_0 = 24\text{nm}$. Other parameters are the same as Fig. 2(a). The red dashed lines denote the DPs' locations. The scattering diagrams in (f) are the shift of DPs with $w_A = 45\text{nm}$, $w_B = 30\text{nm}$ and $w_A = 60\text{nm}$, $w_B = 30\text{nm}$. The line are values calculated by Eq. (16) and average of $f(x)$.

as a special potential and introduces the characters of new DPs [6, 7] into CGSLs. Hence, CGSLs can be regarded as a platform to use new DPs' properties [20].

We also plot the ratio of effective Fermi velocity between flat and curved GSLs in Fig. 2 (d). Here, we use v_x and v_y to indicate Fermi velocity in CGSLs. In flat GSLs, x -direction Fermi velocity maintains v_f and y -direction one decreases to v_{y0} . It is demonstrated that with increasing a_0 and fixed T_f , the ratio $\frac{v_x}{v_f}$ and $\frac{v_y}{v_{y0}}$ are both decreased, and $\frac{v_x}{v_f}$ is approximately equal to $\frac{1}{\overline{f(x)}}$. The $\frac{v_y}{v_{y0}}$ is nearly equal to it firstly, but the distinctions between them increase dramatically with large a_0 . These distinctions may be originated from the variation of $f(x)$, which increases with a_0 . The continuous variation of curved surface can produce an effective potential and it has been derived in helicoidal graphene [40]. Fig. 2 (d) also suggests that above relations are also robust against with $V_{A,B}$ and $w_{A,B}$. Therefore, the influences of curvature can be represented partially by $\overline{f(x)}$ sometimes.

Then we move to asymmetric potentials with $w_A \neq w_B$, and band structures are obtained in Fig. 3. The most obvious feature in these figures is that DPs are shifted. From previous research, the DPs' locations in flat CGLs should be at 30meV , 20meV and 16.7meV

[8] under the condition shown by Figs. 3 (a)-(c), (d) and (e) respectively. Thus, DPs move to higher energy when $w_A > w_B$ in Figs. 3 (a)-(c). Opposite conclusion can be seen in Figs. 3 (c)(d) when $w_A < w_B$. This is because that $f(x)$ has larger value in A than B region with $w_A > w_B$ (shown by Fig. 1(c)) and is opposite with $w_A < w_B$. Comparing Figs. 3 (b)(c) or (d)(e), one can also find that displacements of DPs also increase with increasing a_0 and $w_{A(B)}$.

To understand the robustness or shift of DPs induced by space-dependent Fermi velocity in different conditions, we propose a simplified theoretical model here. We set $f(x)$ in each potential A or B is constant $f_{A(B)}$ and $T_f = \Lambda$. Since the average of $f(x)$ can reflect some effects of curvature, we set $f_{A(B)}$ as it in the range of the potential. Then Eq. (11) reduces to

$$\begin{aligned} \cos(\beta_x \Lambda) = & \cos(q_A w_A + q_B w_B) \\ & + \frac{\cos(\theta_A - \theta_B) - 1}{\cos \theta_A \cos \theta_B} \sin(q_A w_A) \sin(q_B w_B), \end{aligned} \quad (14)$$

with $q_{A(B)}^2 = (f_{A(B)} k_{A(B)})^2 - (f_{A(B)} k_y)^2$. From previous analysis, when $V_B < E < V_A$, the DPs in $k_y = 0$ should exist and the locations are decided by $q_A w_A = -q_B w_B$ [8]. With $k_y = 0$, it should be $f_A k_A w_A = -f_B k_B w_B$. Substituting the expression of $k_{A(B)}$, we get the DP's location

$$E = \frac{f_A w_A V_A + f_B w_B V_B}{f_A w_A + f_B w_B}. \quad (15)$$

When $f_A = f_B = 1$, Eq. (15) reduces to the flat one. When $f_A \neq f_B$, the locations of DPs may shift, and the displacement from flat situation Δ reads

$$\Delta = \frac{(f_A - f_B)(V_A - V_B)w_A w_B}{(f_A w_A + f_B w_B)(w_A + w_B)}. \quad (16)$$

In Fig. 2, $f(x)$ has the same value in potential A and B since $w_A = w_B$, which corresponds to $f_A = f_B$ and $\Delta = 0$. In Figs. 3 (b) and (c), $f_A > f_B$ and $V_A > V_B$, then $\Delta > 0$ and DPs shift to the higher energy. Figs. 3 (d) and (e) are opposite. Meanwhile, Eq. (16) also states that Δ is proportion to $w_{A,B}$, which is also consistent with the conclusion gained by comparing Figs. 3 (d)(e).

In Fig. 3(f), the changes of DPs' positions with different a_0 and Λ are demonstrated by the scattering diagrams. One can immediately find that with increasing a_0 and Λ , the DPs shift more, which agrees with Eq. (16) and suggests their tunability. We also computed the shift from the simplified model with $f(x)$ and Eq. (16). These results are shown by the lines and fit the realistic ones well. Therefore, constructing CGSLs can be a feasible way to tune the locations of DPs by adjusting both potentials and curved surfaces. Other ways that can change Fermi velocity [19, 53–55] are also possible to tune DPs. Furthermore, one may need to concentrated

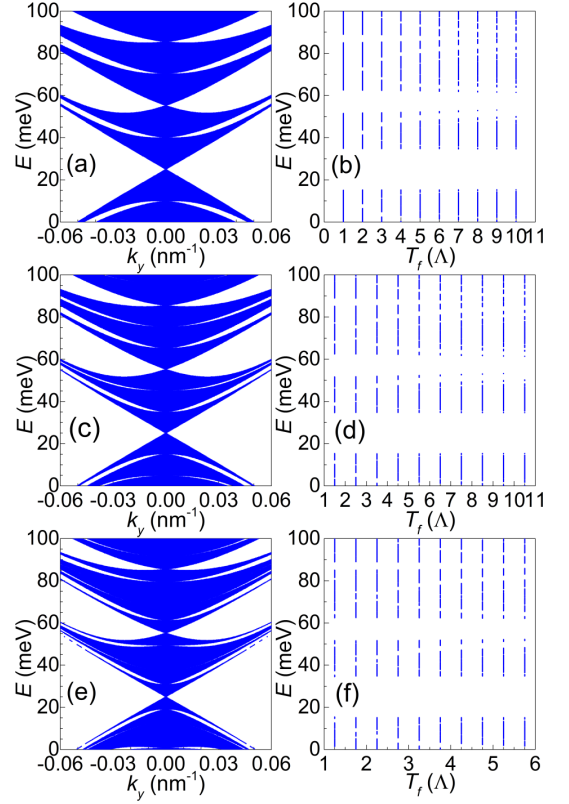


FIG. 4. (Color online) Band structures when $T_f = 2\Lambda$ (a), 1.5Λ (c) and 1.25Λ (e) with $a_0\alpha = \frac{\pi}{4}$. (b), (d) and (f) show the electronic states in different T_f and E with fixed $k_y = 0.02\text{nm}^{-1}$ and $a_0\alpha = \frac{\pi}{4}$. Other parameters are the same as Fig. 2(a).

on these effects in experiments since the intrinsic feature [26] of ripples in graphene and potentials may be not strictly symmetric.

Next we will discuss the condition for $T_f > \Lambda$. Here we plot band structures when $T_f = 2\Lambda$, 1.5Λ and 1.25Λ in Figs. 4 (a) (c) and (e). For analyzing the impacts of periods, we would like to fix the amplitude of $f(x)$. Note that $f(x)$ has period dependent amplitude, we should change a_0 and T_f simultaneously to make $a_0\alpha$ fixed. We choose $a_0\alpha = \frac{\pi}{4}$, which is the same with Fig. 2(b). Therefore, the locations of DPs and slope of bands are the same in these figures, but there are some new gaps in band structures. Besides, the number of gaps increases from Fig. 4 (a)-(e). That means two different periods construct aperiodic structures with various orders. The robustness of locations of DPs are also the same as aperiodic GSLs [11]. Then we plot the electronic states versus different T_f and find that with increasing T_f , the number of new gaps clearly increases, which means the order of aperiodic structures increases. These new gaps are also controllable by adjusting T_f . When T_f is larger than a specific value, the energy bands become the discontinuous ones. Our results propose another way

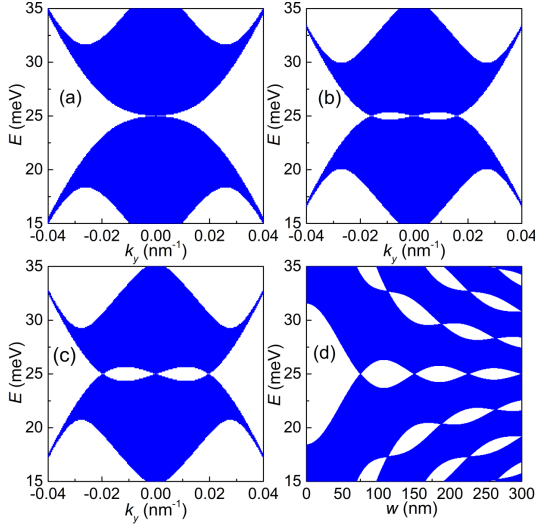


FIG. 5. (Color online) Electronic band structures when $a_0 = 0$ (a), 40nm(b) and 50nm(c) with $w_A = w_B = 80$ nm and $T_f = \Lambda$. (d) is dependence of band structures on periods of potentials with fixed $k_y = 0.01\text{nm}^{-1}$ and $a_0\alpha = \frac{\pi}{4}$. Here $w_A = w_B = w$ and $T_f = \Lambda = 2w$. Other parameters are the same as Fig. 2(a).

to construct aperiodic GSLs and acquire tunable band gaps by changing T_f . Meanwhile, curved graphene in experiments may be not exactly periodic [27], so there may be some gaps in realistic CGSLs.

Previous studies reveal that new DPs locate at $k_y \neq 0$ could appear with some condition in flat GSLs [4–7], such as large lattice constants or potentials. Now we discuss the condition for the appearance of new DPs in CGSLs. We still consider the simplest situation $w_A = w_B$ and $T_f = \Lambda$.

We firstly increase the periods of potentials to obtain new DPs. In Figs. 5 (a)-(c), we plot band structures with $w_A = w_B = 80$ nm and $a_0 = 0, 30$ nm and 40nm. It is demonstrated that the slopes of band structures decrease to nearly vanished and then new DPs appear with increasing a_0 . The k_y -direction coordinates of new DPs also increase with increasing a_0 . These results illustrate that space-dependent Fermi velocity makes the existence of new DPs easier. Thus, we plot electronic states with different $w_{A(B)}$. Comparing it and Fig. 5(d) in Ref. [8], it indicates that new DPs can exist with smaller w when $a_0 \neq 0$.

The condition for the existence of new DPs can also be discussed by the simplified model proposed above. It has been illustrated in literatures [7, 8, 23] and Eq. (14) that once the condition

$$q_A w_A = -q_B w_B = m\pi, \quad m = 1, 2, 3, \dots, \quad (17)$$

is satisfied under some specific k_y , $\sin(q_A w_A) = \sin(q_B w_B) = 0$ and $\cos(q_A w_A + q_B w_B) = 1$, then $\cos(\beta_x \Lambda) = 1$ and β_x always has real solution with all

energies. This condition leads to the close of *zero- \bar{k} gap* and a pair of new DPs will appear away from $k_y = 0$. If we set $V_A = -V_B$ and $w_A = w_B$, then $f_A = f_B = f$, the DPs should locate at zero energy, so we discuss $E = 0$ next, which refers to zero-energy modes studied by previous papers [6, 23]. Under above assumption, we obtain

$$k_{y,m} = \pm \sqrt{\left(\frac{V}{\hbar v_f}\right)^2 - \left(\frac{2m\pi}{f\Lambda}\right)^2}, \quad m = 1, 2, 3, \dots, \quad (18)$$

is satisfied with above conditions. The new DPs will exist when $\left(\frac{V}{\hbar v_f}\right)^2 - \left(\frac{2m\pi}{f\Lambda}\right)^2 > 0$. Therefore, when $f > 1$, $k_{y,m}$ can get real solutions with smaller Λ and makes the generation of new DPs easier. This conclusion is consistent with Fig. 5(d).

Eq. (18) can also be changed to

$$k_{y,m} = \pm \frac{2\pi}{\Lambda} \sqrt{l^2 - \left(\frac{m}{f}\right)^2}, \quad m = 1, 2, 3, \dots, \quad (19)$$

with $V_A = -V_B = 2\pi l \frac{\hbar v_f}{\Lambda}$. Here l can represent potential since it is proportion to V_A . In flat GSLs (i.e. $f = 1$), a new pair of new DPs are generated once l is a positive integer number larger than one [7, 23]. In CGSLs, $f > 1$, so new DPs can arise with smaller l .

Fig. 6 is plotted to verify the above conclusions. In Figs. 6 (a)-(d), band structures with different a_0 and fixed $l = 1$ are plotted. Here, we still use symmetric potential and $T_f = \Lambda$. It is illustrated that the slope of band firstly decreases to nearly vanished then a new pair of DPs arise with increasing a_0 . These phenomena are totally different from flat ones with $l = 1$, where the first pair of new DPs just appear. Then we set some l and fixed $a_0 = 15$ nm to calculate the band structures in Figs. 6 (e)-(h), and show appearance of the first and second pair of new DPs. It is demonstrated that new DPs can generate in smaller potential when graphene is curved. For example, there are only three DPs when $l = 2$ in flat GSLs, but five in CGSL with $a_0 = 15$ nm. In addition, the upper row of Fig. 6 suggests that the locations of new DPs can be tuned by a_0 even though with fixed potential or l , which can not be realized in flat GSLs. Eq. (19) also denotes that. By comparing the two rows of Fig. 6, one can also find that the coordinates of new DPs in upper rows are obviously smaller than ones in the low row due to smaller l . Our discussions provide a possible method to adjust the locations of new DPs.

Finally, we would like to talk about the number of DPs under different l and a_0 . We compute the zero-energy electronic states with different k_y and l in Fig. 7. When new DPs appear, states away from $k_y = 0$ will be present in these figures. Referring to flat situation Fig. 7(a), we can indicate l at which new DPs arise in (b) and (c). It is shown that l under this condition is smaller with increasing a_0 . The distinctions between flat and curved

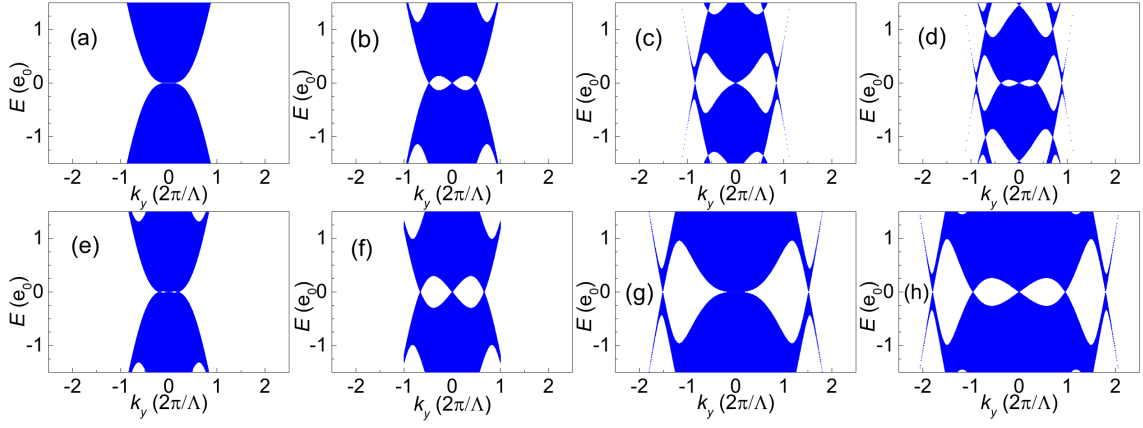


FIG. 6. (Color online) (a)-(d) are electronic band structures with fixed $l = 1$ and $a_0 = 0, 15\text{nm}, 45\text{nm}$ and 55nm respectively. (e)-(h) are the ones with fixed $a_0 = 15\text{ nm}$ and $l = 0.9, 1.1, 1.75$ and 2 respectively. Energy is in units of $e_0 = \frac{\hbar v_f}{\Lambda}$. Other parameters are the same as Fig. 2(a).

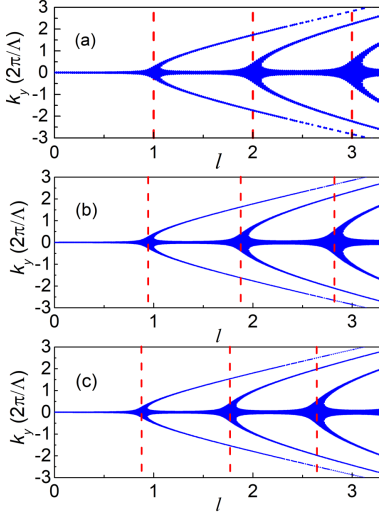


FIG. 7. (Color online) Electronic states in different l and k_y with fixed $E = 0$. Here $a_0 = 0$ (a), $a_0 = 10\text{nm}$ (b) and $a_0 = 15\text{nm}$ (c). Other parameters are the same as Fig. 6. The red dashed lines denote the appearance of new DPs.

ones also increase with larger l . We can conclude that space-dependent Fermi-velocity induced by curvature can arise new DPs with smaller potentials, which means this changed velocity works as an effective potential. This is consistent with analysis above and provides a possible simple way to acquire new DPs and then investigate properties near them. Since above effects are originated from the change of Fermi velocity, our results suggest that forming periodic Fermi-velocity by other ways [19, 53–55] may also be available.

CONCLUSIONS

In summary, we proposed CGSLs by combing curved graphene and periodic potentials with square barriers then investigated their electronic properties. Since we focus on the effects of space-dependent Fermi-velocity, we use Dirac equation in curved spacetime and transfer matrix to gain band structures. For the simplest situation with equal periods and symmetric potentials, the DPs will not move but slopes of bands extremely decrease in both k_x - and k_y -direction. For asymmetric potentials and unequal periods, tunable shifted DPs and extra gaps can appear respectively.

For new DPs, we discussed the condition for their appearance with symmetric potentials and equal periods in detail. The condition for obtaining new DPs can be met more easily when graphene is curved. One can use this property to create new DPs experimentally to investigate physical phenomena near them.

Finally, we would like to emphasize that we reveal part of space-dependent Fermi-velocity's impacts on electronic properties. Although curvature can bring other effects, such as strain and pseudo magnetic field, they are not reflected by our model and need to be analyzed by other means such as tight-binding model with elastic theory. Thus, it is valuable to discuss these effects with more perfect method in the future. Since the ripples in graphene are intrinsic, the effects of them in GSLs should not be neglected in some cases. The controllability of them also provides a new tool to adjust electronic properties in CGSLs.

ACKNOWLEDGMENTS

APPENDIX A. HAMILTONIAN OF CURVED GRAPHENE

Here we refer the process derived by previous research [34] to obtain Hamiltonian with one-dimensional curved surface. According to Eq. (1) and Dirac equation $i\hbar\frac{\partial}{\partial t}\psi = \hat{H}\psi$, we get it in covariant form

$$i\hbar\bar{\gamma}^\mu\partial_\mu\psi = 0, \quad (20)$$

with $\mu = 0, 1, 2$ represents time, x and y coordinate. We first use natural units $v_f = 1$ during calculations. The short lines on the above of $\bar{\gamma}^\mu$ illustrate flat case and $\bar{\gamma}^\mu$ should satisfy anticommutation relation $\{\bar{\gamma}^\mu, \bar{\gamma}^\nu\} = 2\eta^{\mu\nu}I$ with Minkowski metric $\eta_{\mu\nu} = \text{diag}(1, -1, -1)$. $\bar{\gamma}^\mu = (\sigma_3, -i\sigma_2, i\sigma_1)$ with $(\sigma_1, \sigma_2, \sigma_3) = (\sigma_x, \sigma_y, \sigma_z)$ are Pauli matrices. These γ matrices fit above anticommutation relation.

Then we rewrite Eq. (20) into curved case [34], which reads

$$i\hbar\gamma^\mu D_\mu\psi = 0. \quad (21)$$

with metric $g_{\mu\nu}$. There are two differences between curved and flat equations [34] (1) Fielbein fields e_μ^a need to be introduced to indicate the change of γ^μ , which is $\gamma^\mu = e_\mu^a\bar{\gamma}^a$. Here the symbols without short lines mean curved case. Fielbein should fit conditions that $g_{\mu\nu} = \eta_{ab}e_\mu^ae_\nu^b$, γ^μ calculated from Fielbein should have $\{\gamma^\mu, \gamma^\nu\} = 2g^{\mu\nu}I$ and the determinants of metrics are $[\det(g_{\mu\nu})]^{1/2} = \det(e_\mu^a)$. (2) Differential operator should be $D_\mu = \partial_\mu + \Omega_\mu$ and spin connection is

$$\Omega_\mu = \frac{1}{4}e^{\nu a}(\partial_\mu e_\nu^b - \Gamma_{\mu\nu}^\lambda e_\lambda^b)\bar{\gamma}_a\bar{\gamma}_b, \quad (22)$$

with Christoffel symbol $\Gamma_{\mu\nu}^\lambda = \frac{1}{2}g^{\sigma\lambda}(\frac{\partial g_{\nu\sigma}}{\partial x^\mu} + \frac{\partial g_{\mu\sigma}}{\partial x^\nu} - \frac{\partial g_{\mu\nu}}{\partial x^\sigma})$.

After substituting Eq. (3), we gain that

$$e_\mu^a = \text{diag}(1, \sqrt{1+g^2(x)}, 1), \quad (23)$$

and $\Omega_\mu = 0$. After substituting them into Eq. (21), multiplying σ_z in both sides of equation and adding v_f , we obtain Eq. (4).

APPENDIX B. TRANSFER MATRIX FOR CGSL

After acting Eq. (6) on $\Psi = (\tilde{\psi}_A, \tilde{\psi}_B)^T = (\psi_A, \psi_B)^T e^{ik_y y}$, we can get

$$\begin{cases} \frac{1}{f(x)}\frac{d}{dx}\psi_A - k_y\psi_A = ik\psi_B \\ \frac{1}{f(x)}\frac{d}{dx}\psi_B + k_y\psi_B = ik\psi_A \end{cases}, \quad (24)$$

where $k = \frac{E-V(x)}{\hbar v_f}$ is the wave vectors inside potentials. Due to the square barriers of potentials, $V(x)$ in m th

potential region maintains constant V_m . Next we divide the potential region into n parts so $f(x)$ changes little inside each part, then $f(x)$ in the j th part can be regarded as constant f_j . With this approximation, Eq. (24) turns to

$$\begin{cases} \frac{d^2}{dx^2}\psi_A + f_j^2(k_j^2 - k_y^2)\psi_A = 0 \\ \frac{d^2}{dx^2}\psi_B + f_j^2(k_j^2 - k_y^2)\psi_B = 0 \end{cases}. \quad (25)$$

The following processes will be the same as Ref. [8].

* txma@bnu.edu.cn

† sxwlg@yahoo.com

- [1] K. S. Novoselov, A. K. Geim, S. V. Morozov, D. Jiang, Y. Zhang, S. V. Dubonos, I. V. Grigorieva, and A. A. Firsov, *Science* **306**, 666 (2004).
- [2] A. H. Castro Neto, F. Guinea, N. M. R. Peres, K. S. Novoselov, and A. K. Geim, *Rev. Mod. Phys.* **81**, 109 (2009).
- [3] C.-H. Park, L. Yang, Y.-W. Son, M. L. Cohen, and S. G. Louie, *Nat. Phys.* **4**, 213 (2008).
- [4] C.-H. Park, L. Yang, Y.-W. Son, M. L. Cohen, and S. G. Louie, *Phys. Rev. Lett.* **101**, 126804 (2008).
- [5] C.-H. Park, Y.-W. Son, L. Yang, M. L. Cohen, and S. G. Louie, *Phys. Rev. Lett.* **103**, 046808 (2009).
- [6] L. Brey and H. A. Fertig, *Phys. Rev. Lett.* **103**, 046809 (2009).
- [7] M. Barbier, P. Vasilopoulos, and F. M. Peeters, *Phys. Rev. B* **81**, 075438 (2010).
- [8] L.-G. Wang and S.-Y. Zhu, *Phys. Rev. B* **81**, 205444 (2010).
- [9] S. Dubey, V. Singh, A. K. Bhat, P. Parikh, S. Grover, R. Sensarma, V. Tripathi, K. Sengupta, and M. M. Deshmukh, *Nano Lett.* **13**, 3990 (2013).
- [10] C. Bai and X. Zhang, *Phys. Rev. B* **76**, 075430 (2007).
- [11] T. Ma, C. Liang, L.-G. Wang, and H.-Q. Lin, *Applied Physics Letters* **100**, 252402 (2012).
- [12] H. Cheng, C. Li, T. Ma, L.-G. Wang, Y. Song, and H.-Q. Lin, *Applied Physics Letters* **105**, 072103 (2014).
- [13] Y. Xu, J. Zou, and G. Jin, *Journal of Physics: Condensed Matter* **25**, 245301 (2013).
- [14] Q. Zhao, J. Gong, and C. A. Müller, *Phys. Rev. B* **85**, 104201 (2012).
- [15] L. Dell'Anna and A. De Martino, *Phys. Rev. B* **79**, 045420 (2009).
- [16] L. Dell'Anna and A. De Martino, *Phys. Rev. B* **83**, 155449 (2011).
- [17] F. Zhai and K. Chang, *Phys. Rev. B* **85**, 155415 (2012).
- [18] D. Moldovan, M. Ramezani Masir, L. Covaci, and F. M. Peeters, *Phys. Rev. B* **86**, 115431 (2012).
- [19] F. M. D. Pellegrino, G. G. N. Angilella, and R. Pucci, *Phys. Rev. B* **85**, 195409 (2012).
- [20] J. Luan, S. Li, T. Ma, and L.-G. Wang, *Journal of Physics: Condensed Matter* **30**, 395502 (2018).
- [21] A. Isacsson, L. M. Jonsson, J. M. Kinaret, and M. Jonson, *Phys. Rev. B* **77**, 035423 (2008).
- [22] S. Rusponi, M. Papagno, P. Moras, S. Vlaic, M. Etzkorn, P. M. Sheverdyaeva, D. Pacilé, H. Brune, and C. Carbone, *Phys. Rev. Lett.* **105**, 246803 (2010).

- [23] X. Fan, W. Huang, T. Ma, and L.-G. Wang, *Phys. Rev. B* **93**, 165137 (2016).
- [24] Y. Cao, V. Fatemi, A. Demir, S. Fang, S. L. Tomarken, J. Y. Luo, J. D. Sanchez-Yamagishi, K. Watanabe, T. Taniguchi, E. Kaxiras, R. C. Ashoori, and P. Jarillo-Herrero, *Nature* **556**, 80 (2018).
- [25] Y. Cao, V. Fatemi, S. Fang, K. Watanabe, T. Taniguchi, E. Kaxiras, and P. Jarillo-Herrero, *Nature* **556**, 43 (2018).
- [26] A. Fasolino, J. H. Los, and M. I. Katsnelson, *Nature Materials* **6**, 858 (2007).
- [27] L. Tapasztó, T. Dumitrică, S. J. Kim, P. Nemes-Incze, C. Hwang, and L. P. Biró, *Nat. Phys.* **8**, 739 (2012).
- [28] A. L. Vázquez de Parga, F. Calleja, B. Borca, M. C. G. Passeggi, J. J. Hinarejos, F. Guinea, and R. Miranda, *Phys. Rev. Lett.* **100**, 056807 (2008).
- [29] W. Bao, F. Miao, Z. Chen, H. Zhang, W. Jang, C. Dames, and C. N. Lau, *Nature Nanotechnology* **4**, 562 (2009).
- [30] H. Yan, Z.-D. Chu, W. Yan, M. Liu, L. Meng, M. Yang, Y. Fan, J. Wang, R.-F. Dou, Y. Zhang, Z. Liu, J.-C. Nie, and L. He, *Phys. Rev. B* **87**, 075405 (2013).
- [31] G.-X. Ni, Y. Zheng, S. Bae, H. R. Kim, A. Pachoud, Y. S. Kim, C.-L. Tan, D. Im, J.-H. Ahn, B. H. Hong, and B. Özyilmaz, *ACS Nano* **6**, 1158 (2012).
- [32] G. X. Ni, H. Wang, J. S. Wu, Z. Fei, M. D. Goldflam, F. Keilmann, B. Özyilmaz, A. H. Castro Neto, X. M. Xie, M. M. Fogler, and D. N. Basov, *Nature Materials* **14**, 1217 (2015).
- [33] W.-H. Park, I. Jo, B. H. Hong, and H. Cheong, *Nanoscale* **8**, 9822 (2016).
- [34] M. Vozmediano, M. Katsnelson, and F. Guinea, *Physics Reports* **496**, 109 (2010).
- [35] B. Amorim, A. Cortijo, F. de Juan, A. Grushin, F. Guinea, A. Gutiérrez-Rubio, H. Ochoa, V. Parente, R. Roldán, P. San-Jose, J. Schiefele, M. Sturla, and M. Vozmediano, *Physics Reports* **617**, 1 (2016).
- [36] F. de Juan, A. Cortijo, and M. A. H. Vozmediano, *Phys. Rev. B* **76**, 165409 (2007).
- [37] F. de Juan, M. Sturla, and M. A. H. Vozmediano, *Phys. Rev. Lett.* **108**, 227205 (2012).
- [38] A. J. Chaves, T. Frederico, O. Oliveira, W. de Paula, and M. C. Santos, *Journal of Physics: Condensed Matter* **26**, 185301 (2014).
- [39] E. Arias, A. R. Hernández, and C. Lewenkopf, *Phys. Rev. B* **92**, 245110 (2015).
- [40] V. Atanasov and A. Saxena, *Phys. Rev. B* **92**, 035440 (2015).
- [41] M. Watanabe, H. Komatsu, N. Tsuji, and H. Aoki, *Phys. Rev. B* **92**, 205425 (2015).
- [42] P. Castro-Villarreal and R. Ruiz-Sánchez, *Phys. Rev. B* **95**, 125432 (2017).
- [43] F. Guinea, M. I. Katsnelson, and M. A. H. Vozmediano, *Phys. Rev. B* **77**, 075422 (2008).
- [44] M. P. López-Sancho and L. Brey, *Phys. Rev. B* **94**, 165430 (2016).
- [45] T. Kiryu and M. Koshino, *Phys. Rev. B* **99**, 085443 (2019).
- [46] N. Levy, S. A. Burke, K. L. Meaker, M. Panlasigui, A. Zettl, F. Guinea, A. H. C. Neto, and M. F. Crommie, *Science* **329**, 544 (2010).
- [47] F. de Juan, J. L. Mañes, and M. A. H. Vozmediano, *Phys. Rev. B* **87**, 165131 (2013).
- [48] A. A. Pacheco Sanjuan, Z. Wang, H. P. Imani, M. Vanević, and S. Barraza-Lopez, *Phys. Rev. B* **89**, 121403 (2014).
- [49] B. Yang, *Phys. Rev. B* **91**, 241403 (2015).
- [50] K. Flouris, M. Mendoza Jimenez, J.-D. Debus, and H. J. Herrmann, *Phys. Rev. B* **98**, 155419 (2018).
- [51] P. R. Wallace, *Phys. Rev.* **71**, 622 (1947).
- [52] F. M. Toyama and Y. Nogami, *Phys. Rev. A* **59**, 1056 (1999).
- [53] C. Attacalite and A. Rubio, *physica status solidi (b)* **246**, 2523 (2009).
- [54] A. Raoux, M. Polini, R. Asgari, A. R. Hamilton, R. Fazio, and A. H. MacDonald, *Phys. Rev. B* **81**, 073407 (2010).
- [55] P. M. Krstajić and P. Vasilopoulos, *Journal of Physics: Condensed Matter* **23**, 135302 (2011).